Bulletin of the Seismological Society of America, Vol. 93, No. 6, pp. 2434–2444, December 2003

Using *S*/*P* Amplitude Ratios to Constrain the Focal Mechanisms of Small Earthquakes

by Jeanne L. Hardebeck* and Peter M. Shearer

Abstract We test whether *S*-wave/*P*-wave amplitude ratio data can improve the computed focal mechanisms of small earthquakes, using events from two southern California aftershock sequences. The observed *S*/*P* ratios are generally consistent with the expected mechanisms, implying that *S*/*P* ratios can in fact be useful in constraining the focal mechanisms of small events. However, we also find that noise in the observations leads to scatter in the *S*/*P* ratios of factors of 2, and sometimes higher. This scatter limits the usefulness of the *S*/*P* ratios in two ways: (1) the focal mechanism cannot simply be fit to *S*/*P* amplitude data alone without accounting for the noise in a more sophisticated focal mechanism inversion process; (2) while the amplitude ratios may improve poorly constrained mechanisms, they are less useful in refining solutions that are already relatively well constrained.

Introduction

The focal mechanisms of small ($M < 4$) earthquakes can be used to infer the structure and kinematics of faults at depth and to constrain the crustal stress field in which the earthquakes occur. It is therefore important to determine mechanisms for small events as accurately as possible. These mechanisms are most often found using *P*-wave first-motion polarities recorded at local seismic stations. Each observed *P* arrival is mapped to the orientation at which the ray left the focal sphere, and nodal planes are fit to the set of observations (e.g., Reasenberg and Oppenheimer, 1985; Hardebeck and Shearer, 2002).

A number of studies have also used *S*/*P* amplitude ratios (e.g. Kisslinger, 1980; Kisslinger *et al.*, 1981; Julian and Foulger, 1996; Rau *et al.*, 1996; Shen *et al.*, 1997) or absolute *P* and *S* amplitudes (e.g., Ebel and Bonjer, 1990; Rögnvaldsson and Slunga, 1993; Schwarz, 1995; Nakamura *et al.*, 1999) to determine focal mechanisms. Systematic variations in *S*/*P* amplitude ratios are expected because *P*-wave amplitudes are large near the *P* and *T* axes of the focal mechanism and smaller near the *P* nodal planes, whereas the *S*-wave amplitudes are largest near the nodal planes. One advantage to using amplitude data is the increase in the number of observations per earthquake. Another advantage is that amplitudes have a range of values, not the simple binary up or down of the *P*-wave first motions, and therefore may more precisely constrain the location of a given observation on the focal sphere.

There are a few drawbacks to the use of amplitude data. Several factors besides the source mechanism contribute to the observed amplitude at a station. Corrections must be made for event magnitude, geometrical spreading, attenuation, and station site effects. Using *S*/*P* amplitude ratios simplifies this somewhat, since there is no need for magnitude or geometrical spreading corrections and only the differences between *P*-wave and *S*-wave attenuation and site effects need to be considered. There also may be problems correctly picking the *S* arrivals, and possibly near-nodal *P* arrivals, because of scattered phases (Ebel, 1989; Ebel and Bonjer, 1990), and direct arrivals may be obscured by refracted waves if there are strong lateral seismic velocity gradients (Ben-Zion and Malin, 1991). In addition, choices must be made about how to filter the records and how exactly to measure the amplitude.

Focal mechanisms obtained using amplitude data have been compared with *P*-wave polarity mechanisms and orientations inferred from regional tectonics, and the results are mixed. For example, Kisslinger (1980) found that while a set of focal mechanisms in California was consistent with local tectonics, a set in Germany was incompatible. Ebel and Bonjer (1990) also studied events from the same region of Germany and concluded that the solutions were in good agreement with the *P*-wave polarity mechanisms. Schwartz (1995) found that while the amplitude-based focal mechanisms of some moderate-sized earthquakes in Costa Rica and California are consistent with results from waveform modeling, the solutions for most of the smaller events were not in good agreement with *P*-wave polarity mechanisms. Additionally, Rau *et al.* (1996) and Nakamura *et al.* (1999) have demonstrated that sets of focal mechanisms in Taiwan and

*Present address: U.S. Geological Survey, 345 Middlefield Road, MS 977, Menlo Park, California, 94025.

Japan, respectively, are spatially coherent and consistent with regional tectonics.

More work is therefore needed to determine how well amplitude data constrain the focal mechanisms of small earthquakes. We investigate the use of *P*- and *S*-wave amplitudes in constraining focal mechanisms using data from two aftershock sequences in southern California. Both sequences are particularly well recorded, with good station coverage and high-quality digital records, and many of the events have well-constrained *P*-wave polarity mechanisms. We test if the observed amplitudes are consistent with the known focal mechanisms and whether or not including the amplitude data improves the solutions.

Northridge Aftershocks

To test how well *S*- and *P*-wave amplitudes constrain the focal mechanisms of small earthquakes, we need an earthquake data set for which the correct mechanisms are known. One such data set is a cluster of aftershocks of the 1994 *M* 6.7 Northridge, California, earthquake. All of the events in this cluster have highly similar waveforms, as determined by cross correlation (Shearer *et al.*, 2003), implying that they have very similar locations and mechanisms. The well-constrained *P*-wave first-motion polarity mechanisms for the events are quite similar (Hardebeck and Shearer, 2002) and are in good agreement with the consensus mechanism for the set and the orientation of the plane defined by high-precision relative relocations of the events (Shearer et al., 2003). Therefore we feel confident that the correct mechanism for the cluster is known.

We study 43 earthquakes, *M* 1.4–3.4, from this similar event cluster and 160 additional events, *M* 1.4–4.6, from elsewhere in the Northridge region (Fig. 1). We use waveforms from 4 permanent short-period stations of the Southern California Seismic Network (SCSN), 1 broadband TERRAscope station, and 10 temporary short-period stations deployed by the Southern California Earthquake Center (SCEC) to record the Northridge aftershock sequence. All waveform data were acquired from the SCEC Data Center.

S/*P* Amplitude Ratios

We compute the *S*/*P* amplitude ratio for each three-component seismogram. The velocity seismograms are integrated to displacement and filtered with a bandpass of 1–15 Hz. The *P*-wave amplitude is defined as the peak of the first half-cycle, therefore the direct arrival, and is measured on the Cartesian sum of the radial and vertical components. Since the *S* arrival is more ambiguous because converted phases may arrive before the direct *S* wave (e.g., Ebel, 1989), we take the *S*-wave amplitude to be the maximum amplitude on all three channels within the first 2 sec of the apparent *S* arrival. Only observations with signal-to-noise ratios of at least 3 are used. As discussed later, we find little sensitivity of the results to these measurement choices.

The *S*/*P* amplitude ratio observations must be corrected for site and path effects. An empirical station correction is applied for each of the 15 stations, following Shen *et al.* (1997). We assume that all station site effects are linear, so the correction is simply a scalar offset to the observed log(*S*/*P*) value. The empirical station corrections should also approximately correct for path attenuation effects, since most attenuation occurs in the shallow crust and is therefore near receiver.

To determine the station corrections, we consider the 160 events occurring throughout the Northridge aftershock zone (Fig. 1). The diversity of the locations and mechanisms (Shearer *et al.*, 2003) of these events ensures that the observations at each station provide a relatively unbiased sampling of the focal sphere. The station correction is the shift necessary for the mean observed log(*S*/*P*) at that station to match the theoretical mean for a uniform sampling of the focal sphere. The distribution of corrected log(*S*/*P*) values closely matches the theoretical distribution (Fig. 2). This supports the assumption that each station adequately samples the focal sphere and demonstrates that the variation in the observed values is consistent with that expected if the *S*/*P* ratio is primarily controlled by the focal mechanism.

The *S*/*P* ratios for the earthquakes in a similar event cluster should be the same and consistent with the known focal mechanism for the cluster. The average corrected log(*S*/*P*) values for the set of Northridge similar events are qualitatively consistent with the preferred focal mechanism for the set based on the consensus *P*-wave polarities (Fig. 3). As expected, relatively low log(*S*/*P*) values are observed at stations SMIP, SSAP, MPKP, and CPCP, which fall near the middle of the compressional quadrant of the focal mechanism. Stations falling near the *P* nodal planes, such as CALB, SYL, LA00, and LA01, have higher average log(*S*/*P*). While the amplitude ratios are on average in agreement with the known focal mechanism, there are considerable amplitude variations at many of the stations.

Since the *S*/*P* ratios for the similar events should be the same, the scatter in the *S*/*P* ratios at each station provides a measure of the observational noise. The scatter (root mean square [rms] difference from the log mean) in amplitude ratios is usually a factor of 2, but for some stations it is up to a factor of 7. This scatter is not significantly reduced by changing the measurement parameters, such as the frequency passband, as discussed later. Small variations in the focal mechanisms also do not adequately explain the variations in the observed *S*/*P* ratios. This and other possible explanations for the scatter will be explored later; for now we will simply consider it to be noise.

Using Amplitude Ratios to Constrain Focal Mechanisms

Next we include the corrected amplitude ratios in the focal mechanism inversion and test whether this improves the solutions. We try two approaches, both based on the *P*-wave polarity inversion technique introduced by Hardebeck and Shearer (2002). This method determines the stability of

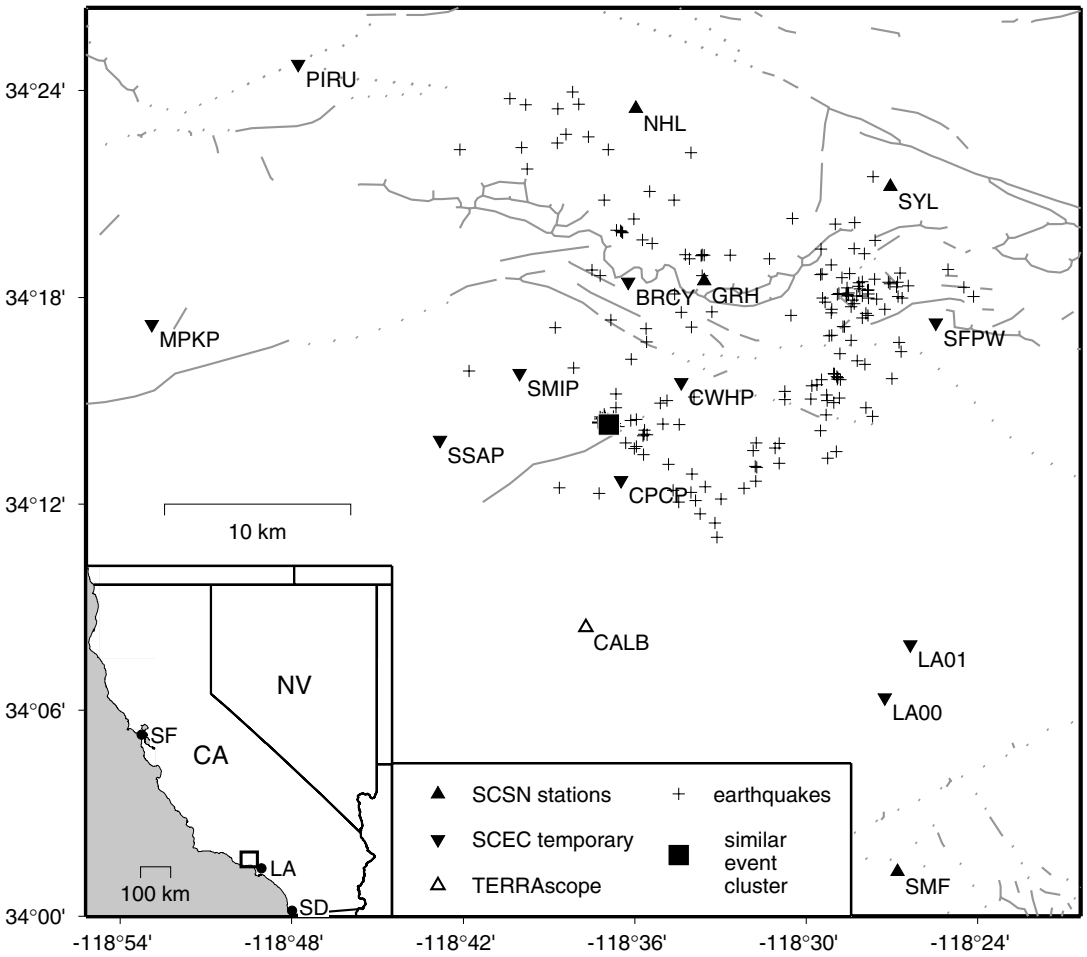

Figure 1. Map of the Northridge region, California. Crosses mark the epicenters of 203 earthquakes used in this study, and the square indicates the location of the similar event cluster. Stations are marked by triangles. Open triangle, TERRAscope permanent broadband station; upright filled triangles, short-period permanent SCSN stations; inverted filled triangles, short-period SCEC portable stations. Gray lines indicate mapped fault traces from Jennings (1975). Box in inset map shows location. CA, California; NV, Nevada; LA, Los Angeles; SD, San Diego; SF, San Francisco.

focal mechanism solutions by performing repeated trials with different possible event locations and seismic velocity models. For each event, a set of acceptable mechanisms is generated, composed of solutions that fit at least a threshold fraction of the polarities for at least one trial. The preferred mechanism is taken to be the average of the set, and only if the acceptable solutions are tightly clustered around the preferred mechanism is the solution considered stable and well constrained.

The first approach to using *S*/*P* data is to select the mechanism from the set of acceptable solutions that minimizes the misfit of the *S*/*P* observations. The set of acceptable mechanisms for each event is computed from the *P*-polarity observations at all SCSN, TERRAscope, and SCEC stations recording the event. We allow up to 10% misfit polarities, the rate of polarity errors for the SCSN found by Hardebeck and Shearer (2002). Event locations and location uncertainties are determined using source-specific station terms (Richards-Dinger and Shearer, 2000). We use a smoothed version of a standard 1D southern California seismic velocity model (Shearer, 1997) and four 1D averages of local 3D velocity models (Hauksson and Haase, 1997; Hauksson, 2000).

From the set of acceptable mechanisms derived from the *P* polarities, we then choose the mechanism that minimizes the L1-norm misfit of the corrected log(*S*/*P*) observations. The theoretical *S*/*P* ratios are calculated assuming a pure double-couple source (Shearer, 1999). The azimuth and takeoff angle for each station are computed using the given 1D velocity model. All arrivals are assumed to be direct arrivals, as the crossover distance between the direct and the refracted phase for the southern California velocity structure is ~120 km, beyond the most distant stations.

Since the mechanisms of the similar events should be

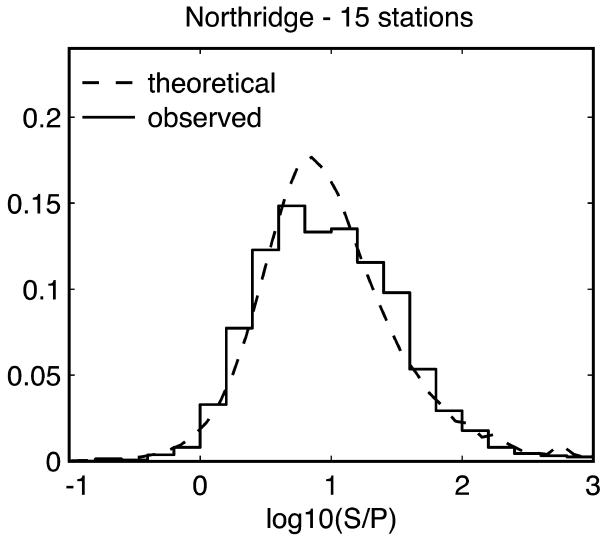

Figure 2. A histogram of the corrected observed *S*/*P* amplitude ratios for 203 Northridge events, recorded at the 15 stations shown in Figure 1. The dashed line shows the theoretical distribution assuming that the observations evenly sample the focal sphere. An empirical station correction, the shift in log(*S*/*P*) necessary to match the mean observed and theoretical values, was applied to the data for each station.

nearly identical, we will consider the addition of the *S*/*P* data to be successful if the mechanisms are more similar than those based on *P*-wave polarity data alone. However, a comparison between the solutions with and without the *S*/*P* ratio data (Fig. 4a–d) reveals that the inclusion of amplitude information has reduced the similarity of the mechanisms. For this example, the amplitude ratio information has degraded, rather than improved, the solutions. The amplitude ratios neither help refine reasonably well-constrained mechanisms (quality A and B of Hardebeck and Shearer [2002]), nor constrain poorly determined ones (quality C and D).

The second approach incorporates the uncertainty in the *S*/*P* observations into the focal mechanism inversion, in much the same way as Hardebeck and Shearer (2002) accounted for uncertainty in the *P* polarity data. A new set of acceptable mechanisms is found for each event, and the average of this set is selected as the preferred mechanism. A solution is considered acceptable only if the number of misfit polarities and the total L1-norm log(*S*/*P*) misfit are both below their respective threshold values. An amplitude ratio threshold equivalent to a factor of 2 difference at each station is chosen, corresponding to the observed noise. Other values were also tested, and the results do not appear to be sensitive to the threshold value.

Comparing the mechanisms found using the second method with those from the *P*-wave polarities alone (Fig. 4a,b,e,f) shows that this time the addition of the *S*/*P* ratios has not degraded the solutions and has improved some of the mechanisms. In particular, the events with poorly constrained (quality C and D) *P*-wave polarity solutions benefit from the use of amplitude information. The polarity data alone successfully constrain the *T* axes of the focal mechanisms to be near vertical, but the *P* axes are scattered in all directions. For the solutions incorporating *S*/*P* ratios, however, 10 of the 11 *P* axes are clustered around the correct orientation.

This demonstrates that *S*/*P* data can be used to constrain focal mechanisms. In particular, the inclusion of amplitude information can improve the solutions of events with poor-quality *P*-wave polarity mechanisms. However, the noise in the *S*/*P* observations must be accounted for in the inversion method.

Test Simulating Sparse Data Sets

Most earthquake sequences are recorded by only a few stations, and it is in these regions of sparse coverage that additional data such as *S*/*P* amplitude ratios are most needed. We simulate this situation by using data from only a subset of the stations for the earthquakes of the similar event cluster. For each event, four to eight stations with good-quality *P*-wave polarity and *S*/*P* amplitude ratio observations are randomly chosen, and data from only these stations are used. The experiment is repeated using subsets of 8–12 stations per event. We use the second inversion method presented earlier, where the uncertainties in the amplitude ratios are used in generating the set of acceptable mechanisms.

The focal mechanisms are clearly not well constrained by the *P*-wave polarity data alone. In both cases, the *T* axes are scattered but generally near vertical, while the *P* axes are in all directions (Fig. 5a,c). The addition of the *S*/*P* amplitude data only moderately improves the solutions where four to eight stations are used (Fig. 5b). The majority of *T* axes are more closely clustered, although offset from the correct orientation, and some *P* axes are correctly oriented. In the case where 8–12 stations are used, however, the improvement is considerable (Fig. 5d). The *T* axes are clustered near, but slightly offset from, the correct orientation, and only 4 of the 20 *P* axes are not reasonably close to the correct axis.

Again we find that the *S*/*P* amplitude information can significantly improve the mechanisms of earthquakes with poor-quality *P*-wave polarity solutions. However, it appears that accurate mechanisms generally cannot be found for events with very sparse station coverage, even with the inclusion of amplitude data. A minimum of about eight stations appears to be required.

Anza Aftershocks

Next we study a set of 42 aftershocks, *M* 1.0–2.8, of the *M* 5.1 2001 Anza, California, earthquake. These earthquakes occurred in the densest part of the Anza broadband seismic network (Fig. 6). They are all located within ~1 km of each other, but their waveforms are not highly correlated (Kilb *et al.*, 2002), so we cannot assume that the events have similar mechanisms. The *P*-wave polarity mechanisms, found using

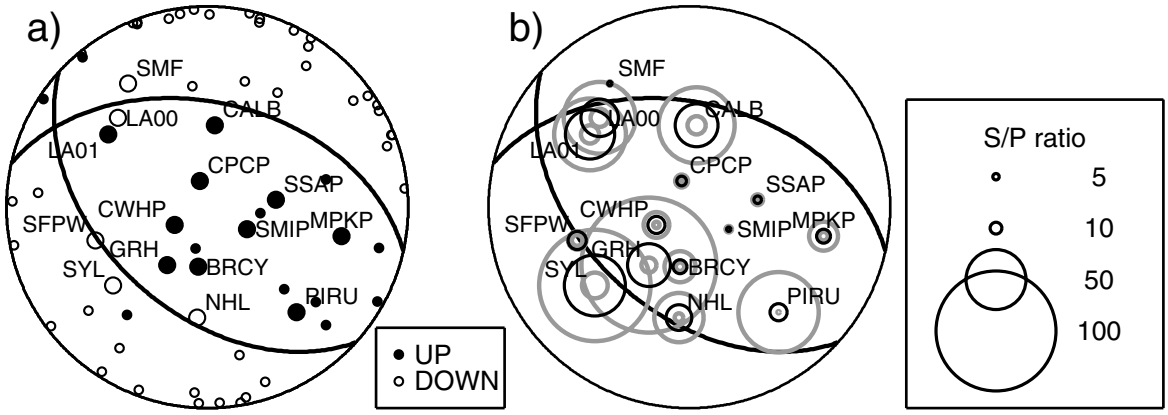

Figure 3. *P*-wave polarities and *S*/*P* ratios for 43 earthquakes of the Northridge similar event cluster, in lower hemisphere stereographic projection. (a) The consensus *P*-wave polarities at all stations recording the events: filled circles, up; open circles, down. The consensus polarity is the polarity observed at a station for the majority of recorded events. The nodal planes represent the consensus *P*-polarity focal mechanism. The stations used for *S*/*P* ratios are shown as larger circles; additional stations contributing *P*-polarity readings are shown as smaller circles. Not all events are recorded at all stations. (b) Station-corrected *S*/*P* amplitude ratios for the 15 stations in Figure 1. The black circles indicate the log mean value of all of the observations at a single station, and the gray circles indicate the middle 80% of the measurements.

the method of Hardebeck and Shearer (2002), suggest that these events fall into two distinct focal mechanism groups (Fig. 7a,c), although the sets of acceptable mechanisms overlap for many of the events in the two groups.

The *S*/*P* ratio is observed for each event at 10 Anza network stations, using the same methodology as used for the Northridge data. Empirical station corrections are found using 155 pre-mainshock events from the whole Anza region (Fig. 6). The distribution of corrected amplitude ratios is again very similar to the theoretical distribution (Fig. 8).

The amplitude ratios for events in set 1 are generally qualitatively consistent with the average *P*-wave polarity mechanism (Fig. 7a,b), with smaller ratios at midquadrant station PFO and larger ratios at near-nodal stations such as SND, WMC, and KNW. The observations for events in set 2 are slightly less consistent; for example, all the *S*/*P* ratios at station SND are larger than the ratios at station PFO, even though the two stations are approximately equidistant from the nodal plane.

Comparing the observed *S*/*P* ratios of the earthquakes in the two sets (Fig. 7c,d), we see that the *S*/*P* ratios are not significantly different. If the *P*-wave polarity mechanisms of the two sets are correct, there should be a significant difference in amplitudes, especially at stations FRD, SND, WMC, and KNW, which are near nodal for set 1. However, the distributions of observations for set 1 and set 2 events overlap considerably at each of these stations.

The *P*-wave polarities divide the events into the two sets based on the polarities at just two stations, FRD and SND. One nodal plane for events in set 1 is well constrained to fall between stations FRD and SND on one side and closeby stations BZN, WMC, and KNW on the other (Fig. 7c). The corresponding nodal plane for events in set 2, however, is not as well constrained by the polarity data. It must lie between stations FRD, SND, and WMC on one side and TRO and PFO on the other; however, there is a large gap (~30°) between these two sets of stations. All nodal planes within this gap are equally acceptable, so the preferred plane of the Hardebeck and Shearer (2002) method falls in the middle of the gap. Other focal mechanism inversion techniques, such as FPFIT (Reasenberg and Oppenheimer, 1985), would also chose a plane near the center of the gap.

An alternative interpretation of the *P*-wave polarity data is that the true nodal plane of the events in set 2 is very similar to that of the events in set 1, just to the other side of stations FRD and SND. This interpretation is more consistent with the observation that the amplitude ratios for the events in the two groups span similar values, and it is more consistent overall with the observed *S*/*P* ratios (Fig. 7e,f). The alternative set 2 mechanism only slightly increases the total polarity misfit from 3% to 4%, which is still an excellent fit to the *P*-wave polarity data.

This example demonstrates the value of amplitude data for seismotectonic studies in which the goal is to understand small-scale fault complexity. From the *P*-wave polarity data alone, there appear to be two distinct sets of mechanisms at this location. The inclusion of the *S*/*P* amplitude ratios, however, reveals that the mechanisms are very similar, although not identical. This leads to a different seismotectonic interpretation, that the active structures in this location are of similar orientation. Without the *S*/*P* ratios, we would have concluded that two significantly different fault orientations were active.

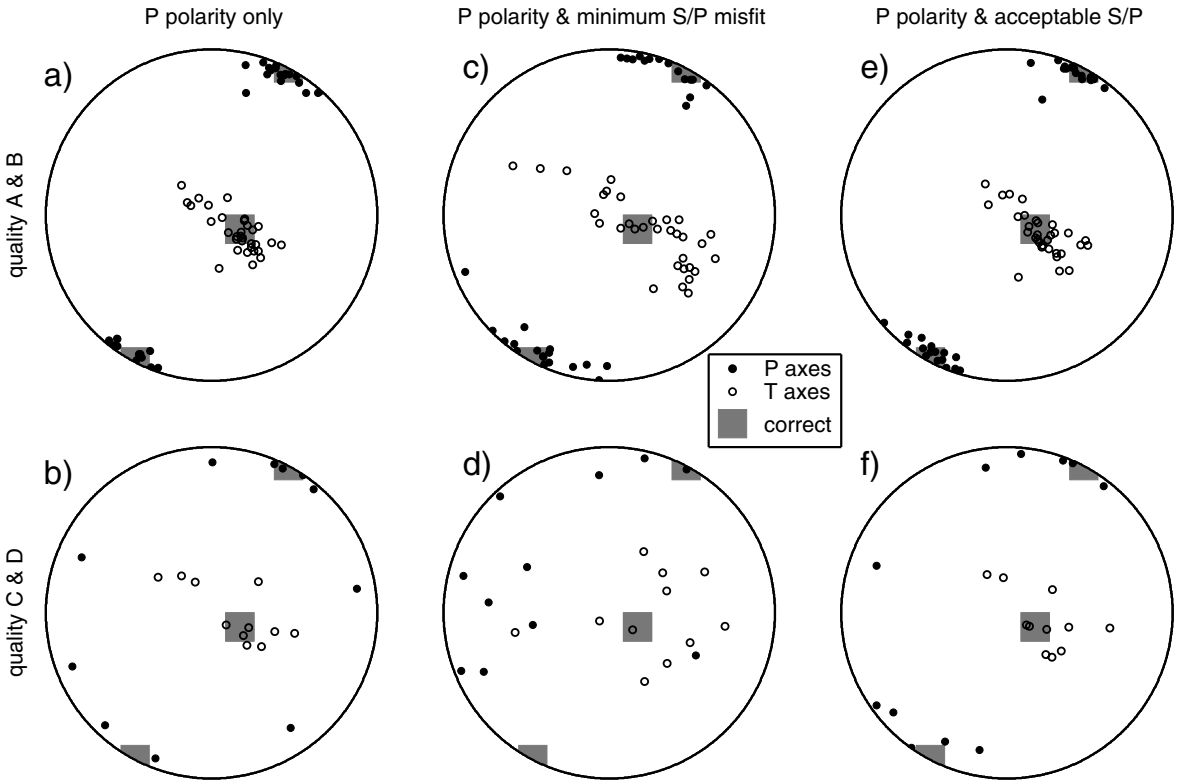

Figure 4. The *P* axes (filled circles) and *T* axes (open circles) of focal mechanisms for the Northridge similar event cluster. The shaded squares indicate the axes for the consensus mechanism (Fig. 3a), assumed to be the correct mechanism. (a) Mechanisms from *P*-polarity data only, found using the technique of Hardebeck and Shearer (2002), for events with high-quality (A and B) *P*-wave polarity solutions. (b) Mechanisms from *P*-polarity data only, low-quality (C and D) solutions. (c) Solutions from *P*-polarity and *S*/*P* ratio observations, for events with high-quality *P*-wave polarity solutions. The *P*-polarity data are used to find a set of acceptable solutions for each event, and the mechanism from this set that minimizes the L1-norm misfit of the observed log(*S*/*P*) is selected. (d) Solutions from *P*-polarity and *S*/*P* ratio observations for events with low-quality *P*-wave polarity solutions. The mechanisms were found as in (c). (e) Solutions from *P*-polarity and *S*/*P* ratio observations, for events with high-quality *P*-wave polarity solutions. The *S*/*P* data are incorporated into the selection of the set of acceptable solutions, allowing only solutions with a total L1-norm log(*S*/*P*) misfit less than a threshold value. The preferred mechanism is the average of the set of acceptable mechanisms. (f) Solutions from *P*-polarity and *S*/*P* ratio observations, for events with low-quality *P*-wave polarity solutions. The mechanisms were found as in (e).

Discussion

Amplitude Ratio Scatter

The observed *S*/*P* ratios for the earthquakes in the Northridge similar event cluster are qualitatively consistent with the preferred mechanism for this cluster, but the observations at a single station usually vary by a factor of 2, sometimes up to a factor of 7. The similar waveforms of these events imply that the locations and mechanisms are very similar, and the observed *S*/*P* ratios at any given station should also be very similar. Here we investigate the potential sources of the observed scatter in the *S*/*P* ratios.

The events are spatially close, with relative relocation indicating that they are within less than 0.5 km of each other, but they are not exactly colocated. Small differences in location translate to differences in takeoff angle and *S*/*P* ratio. We investigate how much of the observed *S*/*P* scatter can be explained by location differences. We allow each event to move up to ± 1 km horizontally and ± 2 km vertically from the average event location, in order to minimize the log(*S*/*P*) amplitude misfit for the preferred mechanism. This results in only a 17% reduction in the L1-norm log(*S*/*P*) misfit, compared to the misfit obtained when the original hypocenters are used. Errors in the velocity model also translate to takeoff angle errors, but introducing a takeoff angle shift at each station reduces the misfit by only 6%. Therefore, location and velocity model errors cannot account for the large scatter in the *S*/*P* observations for our Northridge data

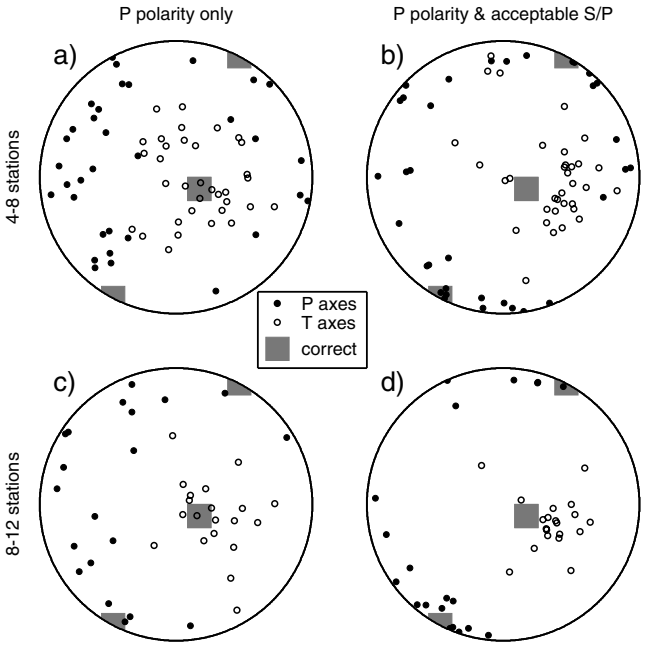

Figure 5. The *P* and *T* axes of focal mechanisms obtained using a subset of the data for the Northridge similar event cluster. For each event, a subset of the stations with good-quality *P*-wave polarities and *S*/*P* ratios were randomly selected to constitute the test data. (a) *P*-wave polarity data only, subsets of four to eight stations. Mechanisms were found as in Figure 4a. (b) *P*-wave polarity and *S*/*P* amplitude ratio data, subsets of four to eight stations. Mechanisms found as in Figure 4e. (c) *P*-wave polarity data only, subsets of 8–12 stations. Mechanisms were found as in Figure 4a. (d) *P*-wave polarity and *S*/*P* amplitude ratio data, subsets of 8–12 stations. Mechanisms found as in Figure 4e.

set. Velocity model errors may become more important if more distant stations are used, however, especially if refracted arrivals are incorrectly modeled.

The events also may not have identical focal mechanisms, and small differences in mechanism lead to differences in the *S*/*P* ratio. We test whether the observed *S*/*P* scatter can be explained by mechanism differences by choosing the mechanism for each event that minimizes the L1-norm log(*S*/*P*) misfit, unrestricted by the *P*-wave polarity data. The total L1-norm log(*S*/*P*) misfit is reduced 38% compared to the case where all of the events are assumed to have the consensus mechanism. This is a larger reduction than achieved by allowing variation in any other parameters. However, an *S*/*P* ratio scatter of a factor of 1.5 is still left unaccounted for. Also, to achieve this misfit reduction, an unacceptable number of the *P* polarity observations are misfit, ~25%, compared to the known ~10% polarity error rate for the Northridge region (Hardebeck and Shearer, 2002). Therefore, there is not a set of focal mechanisms, adequately fitting both the *P* polarity and *S*/*P* ratio data, that does not imply significant scatter in the *S*/*P* observations. This implies that focal mechanism variations alone cannot satisfactorily explain the variability in the *S*/*P* observations.

It is not surprising to find a considerable misfit reduction when the focal mechanisms are allowed to vary, as we have introduced over 100 additional model parameters. We test whether the 38% misfit reduction could have come about simply from increasing the number of model parameters by comparing the results to multiple trials with randomized data. The null hypothesis is that the scatter in the *S*/*P* ratio results from noise unrelated to the focal mechanisms, so we generate test data sets by randomly reassigning the *S*/*P* observations at each station to different events. We then find the best-fitting mechanism for each synthetic event exactly as we did for the real data. We find that 23% of the randomized trials produce misfit reductions greater than 38%. Therefore, we cannot reject the null hypothesis with reasonable certainty, as the misfit reduction may be due solely to increasing the number of model parameters. The misfit reduction of 38% is therefore not conclusive evidence that the scatter in *S*/*P* ratio is due to mechanism variation.

Another possible explanation for the amplitude scatter is that frequency-dependent attenuation has not been adequately corrected for by the simple constant shift of log(*S*/*P*) for each station. If different events have different frequency content, the relative *S* and *P* attenuation may be different and the station correction may underestimate the true correction for some events and overestimate the correction for others. If this were the case, we would expect the misfit of the *S*/*P* ratios to be correlated to event magnitude or stress drop, which we do not observe. Introducing a set of event corrections that subtract the average value for each event reduces the total scatter by only 14%. This rules out a source-related origin of the scatter.

Noise in the amplitude observations can also be explained by the scattering of high-frequency energy. Ebel (1989) found evidence for both near-source and near-receiver scattering affecting the observed amplitudes of high-frequency *P* and *S* waves. However, at least in the Northridge and Anza regions, the scattering is not strong enough to completely obscure the radiation pattern, since the width of the *S*/*P* histogram is correct and the average *S*/*P* ratios do agree with expected mechanisms. We do not know how typical the scattering in the Northridge and Anza regions are of southern California, but they are rapidly deforming areas with complex geological structures. We might expect less scatter in less active and complex regions.

Different amounts of *S*/*P* variation are observed at different stations. This could be related to local differences in geology affecting the level of high-frequency scattering. Converted phases are another possible source of noise for stations situated on sediments. The observations for the Anza network support either converted phases or higher levels of scattering in sedimentary and weathered rock as a source of *S*/*P* variation. The largest *S*/*P* variation (for earthquakes in set 1, which contains the majority of the events) of a factor of ~4 is observed at station WMC, which is lo-

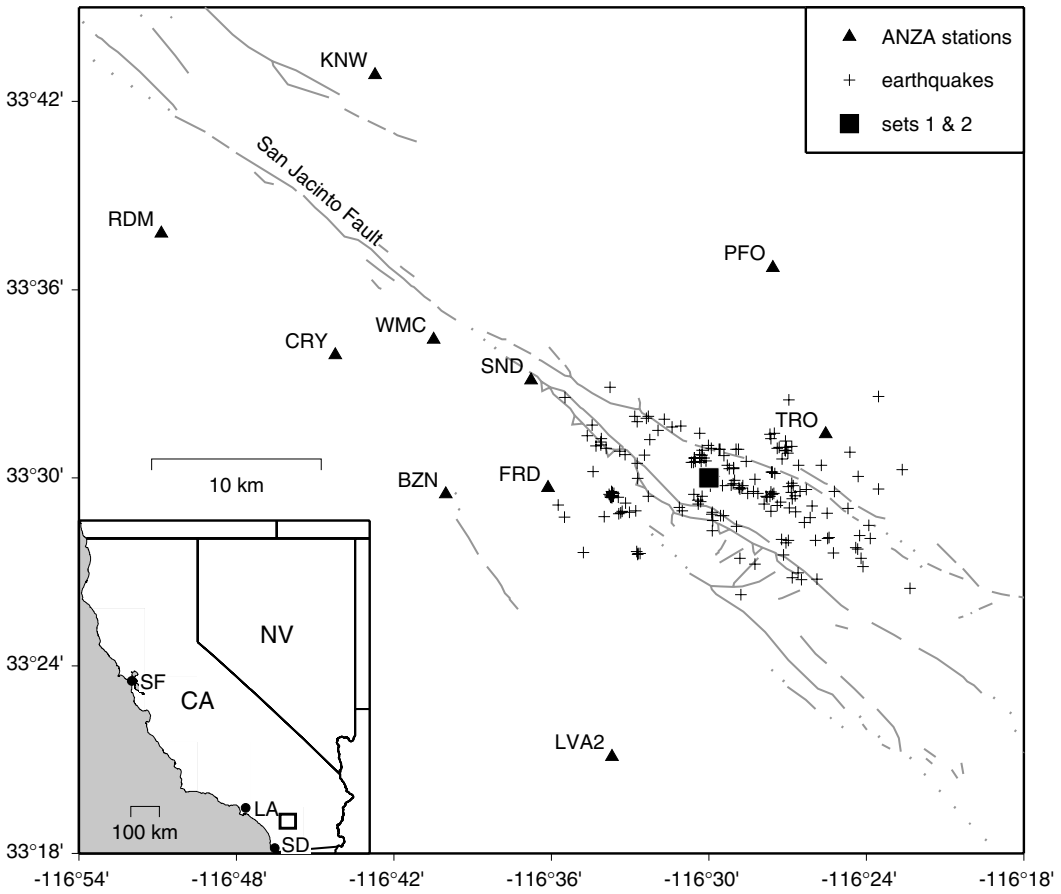

Figure 6. Map of the Anza region, California. Crosses mark the 197 events used, and the square indicates the location of the 42 colocated events of sets 1 and 2. Stations of the broadband Anza seismic network are marked by triangles. Faults from Jennings (1975) as gray lines.

cated on top of ~60 m of alluvium (http://eqinfo.ucsd.edu/deployments/anza.html). The rest of the Anza stations are situated on basement rocks, although sometimes the rock is weathered or decomposed. The second largest *S*/*P* variation, a factor of ~3, is observed at station KNW, above a ~20-m-thick weathering layer.

Most of the Northridge stations are located within sedimentary basins, and the largest *S*/*P* variations, up to a factor of ~7 at station PIRU, are observed there. The five stations situated outside of the basins on rock or stiff soil (BRCY, CALB, LA00, LA01, and SSAP) (Bonilla *et al.*, 1997) have average to low *S*/*P* variations (factors of 1.6–2.1). However, lower variations are also observed at some of the basin stations, such as factors of ~1.3 and ~1.7 at stations SFPW and CPCP, both in the San Fernando Valley, and a factor of ~1.6 at station SMF in the Santa Monica basin. This implies that the variation in *S*/*P* observations is not a simple function of the site conditions.

Some scatter in the *S*/*P* ratios may be introduced if our amplitude measurement choices are not optimal. However, we find that our results are essentially the same and the scatter is not reduced if we change our measurement technique. We have tried using numerous other frequency bands for the seismogram filtering and using the velocity records instead of integrating to displacement. We also tested measuring the *P*- and *S*-wave maximum and rms amplitudes over various time windows and changing the threshold signal-to-noise level. The amount of scatter is also similar if we consider only *P*-wave or only *S*-wave amplitudes without computing their ratio.

The *S*/*P* ratio scatter is a factor of 2–3 for all of the filtering passbands we have tested, spanning 3 orders of magnitude (Fig. 9). Our preferred band of 1–15 Hz results in nearly the lowest level of scatter. We also investigate the average misfit of the *S*/*P* ratios to the best-fitting focal mechanisms as a function of passband. We find that while the average misfit is fairly constant for frequencies greater than ~1 Hz, it increases for lower frequencies, which therefore appear to be dominated by noise unrelated to focal mechanism. For this reason, we have chosen 1 Hz as the lower limit for seismogram filtering.

Thus, the origin of the large scatter in our amplitude observations remains largely unknown. While we can rule out simple explanations involving variations in source lo-

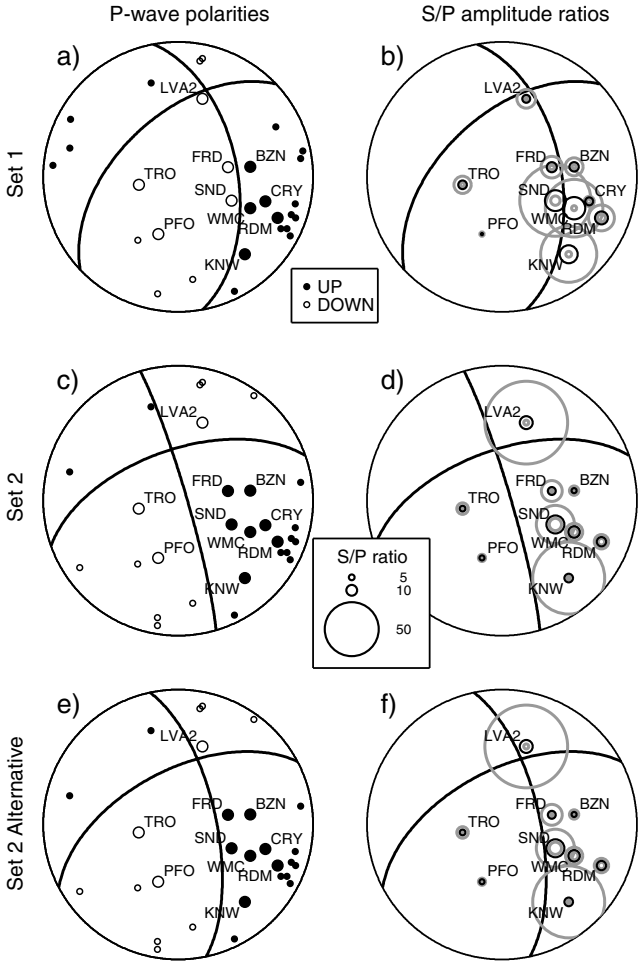

Figure 7. *P*-wave polarities and *S*/*P* ratios for the 42 Anza earthquakes in sets 1 and 2. The events are separated into the two sets based on *P*-wave polarity mechanism. (a) The consensus *P*-wave polarities at all stations recording the 34 events in set 1; symbols as in Figure 3a. The consensus *P*-wave polarity focal mechanism is shown. (b) Observed *S*/*P* ratios for events in set 1, as in Figure 3b. The consensus *P*-wave polarity focal mechanism is shown. (c) The consensus *P*-wave polarities at all stations recording the eight events in set 2; symbols as in Figure 3a. The consensus *P*-wave polarity focal mechanism is shown. (d) Observed *S*/*P* ratios for events in set 2, as in Figure 3b. The consensus *P*-wave polarity focal mechanism is shown. (e) The same as Figure 7c, with an alternative *P*-wave polarity focal mechanism. (f) The same as Figure 7d, with the alternative *P*-wave polarity focal mechanism.

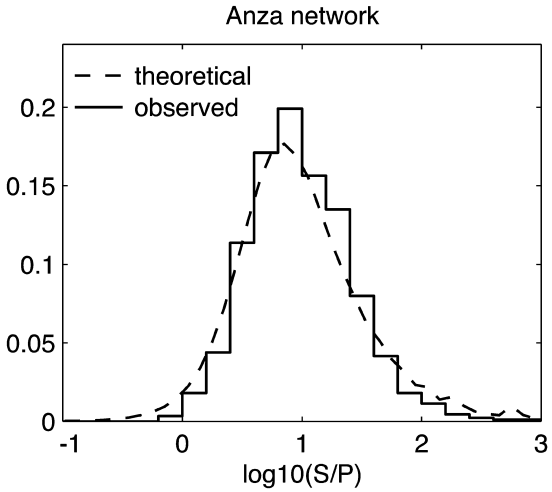

Figure 8. Histogram of the observed *S*/*P* amplitude ratios for 155 Anza region earthquakes, shown in Figure 6, recorded at the stations of the Anza seismic network. The dashed line shows the theoretical distribution assuming that the observations evenly sample the focal sphere. An empirical station correction, the shift in log(*S*/*P*) necessary to match the mean observed and theoretical values, was applied to the data for each station.

cation or mechanism, we have been unable to identify a specific mechanism for generating the scatter. Possibilities include (1) large angular differences in radiated high-frequency seismic energy that are not predicted from double-couple source theory, which might arise from fault-zone irregularities or stress heterogeneity; (2) focusing and defocusing effects caused by small-scale velocity heterogeneity that can produce large amplitude differences among even closely spaced events; and (3) scattering of high-frequency energy in the near-surface rock or sediments.

Effect of Noise on Focal Mechanism Determination

As the scatter in the observed *S*/*P* ratios for the Northridge similar event cluster cannot be attributed to any measurable parameters related to the earthquake source, we consider it to be noise. Assuming that the Northridge events are typical of events recorded by the SCSN, we estimate that the noise in *S*/*P* ratios for that network is typically a factor of 2, but for some stations may be higher. This noise has several implications for the use of *S*/*P* amplitude data in determining earthquake focal mechanisms in southern California.

The first is that the mechanism that best fits the observed *S*/*P* ratios may not be the correct solution, as it is partially fitting noise. This is demonstrated by the poor performance of the focal mechanism inversion method shown in Figure 4c,d, which simply minimizes the misfit of the log(*S*/*P*) values. A more sophisticated scheme is necessary, which takes into account the likely uncertainty in the *S*/*P* observations. One such scheme, shown to be an improvement in Figure 4e,f, is based on the method of Hardebeck and Shearer (2002) and accounts for uncertainty in all input parameters by generating a set of acceptable mechanisms for each event.

Second, while noisy data may be useful in coarsely improving poorly constrained *P*-wave polarity mechanisms, it cannot be used to fine-tune well-constrained mechanisms, as also shown in Figure 4. This should not be too much of a disadvantage, as there are many regions with station coverage less dense than southern California, where focal mech-

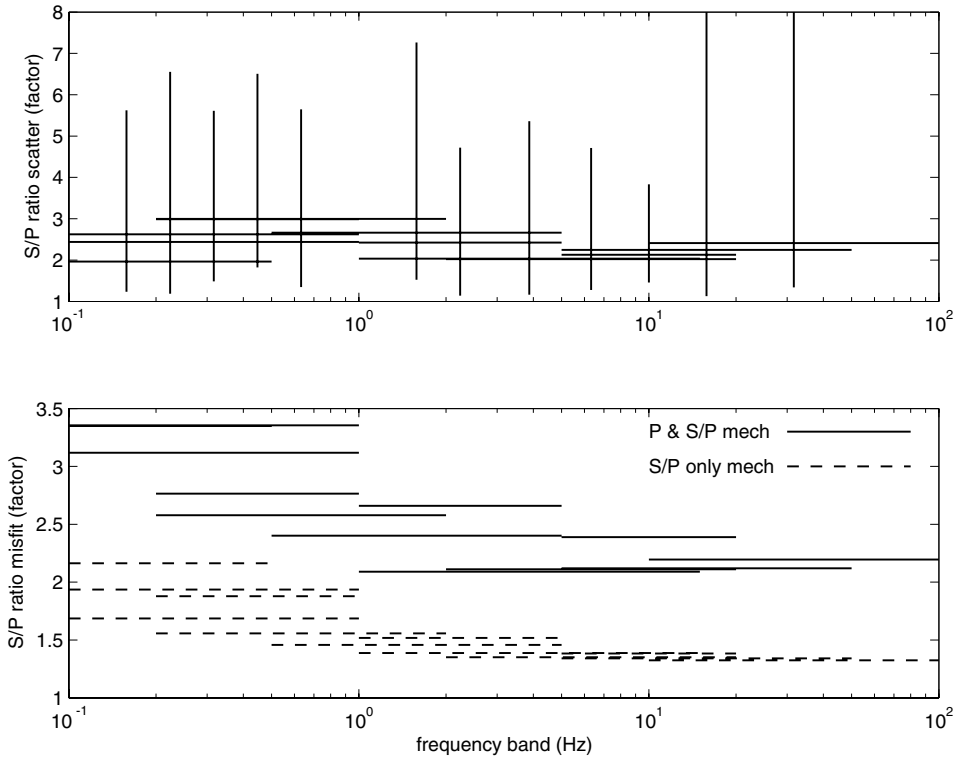

Figure 9. Dependence of the scatter in the observed *S*/*P* ratios on the frequency bandpass used to filter the seismograms. The top panel shows the scatter at the Northridge stations, as a function of passband. The horizontal bar represents the average scatter and shows the bounds of the bandpass, and the vertical bar indicates the range from the station with the least scatter to that with the highest. The lower panel shows the average misfit of the *S*/*P* observations to the best-fitting focal mechanisms. The solid line shows results for mechanisms found from both *S*/*P* ratios and *P*-wave polarities, and the dashed line from *S*/*P* ratios only. The scatter and misfit are both given in terms of "factor," a factor of 2, for example, representing a value either 2 times or 0.5 times the average or predicted value.

anisms could benefit from the addition of *S*/*P* amplitude observations. The tests shown in Figure 5 demonstrate the value of this additional data for events recorded by 8–12 nearby stations, similar perhaps to a temporary deployment for an aftershock sequence.

Conclusions

We have found that the *S*/*P* amplitude ratios measured for small (*M* 1.0–3.4) earthquakes in two aftershock sequences in southern California are generally consistent with the amplitude ratios expected from well-constrained mechanisms based on *P*-wave polarity data. This gives us considerable hope that *S*/*P* ratios can in fact be useful in constraining the focal mechanisms of small events. The improved focal mechanisms for a set of similar events in the Northridge aftershock sequence demonstrate the advantage of using amplitude data in focal mechanism inversions.

However, we also find that the scatter in the observed *S*/*P* ratios at a given station for the set of similar events is typically a factor of 2, sometimes up to a factor of 7. These variations cannot easily be explained by small differences in location or mechanism and therefore represent noise, presumably from scattering. This level of noise means that while amplitude ratios can be useful for determining focal mechanisms, they do have some limitations. First, we cannot simply choose the mechanism that minimizes the *S*/*P* amplitude misfit; we must account for probable noise levels when computing the preferred focal mechanism solution. Second, while the amplitude ratios may improve poorly constrained mechanisms, they probably cannot be used to refine well-constrained solutions.

The example of the Anza aftershock sequence demonstrates the value of amplitude observations for seismotectonics, particularly for studies of small-scale fault complexity. Studying *P*-wave polarity and *S*/*P* amplitude ratio data together, we are able to understand the distribution of fault orientations better than when using *P*-wave polarities alone. Two sets of events that were initially deemed dissimilar based on *P*-wave polarities were found instead to be quite similar.

Acknowledgments

We would like to thank the staff of the SCEC data center, especially Karen Kahler and Rob Clayton, for all their help obtaining the waveform data. We also thank Debi Kilb for helpful discussions and for assistance with the Anza network data. We are grateful to Susan Schwartz and an anonymous reviewer for their comments on the manuscript. This research was supported by the Southern California Earthquake Center. SCEC is funded by NSF Cooperative Agreement EAR-8920136 and USGS Cooperative Agreements 14-08-0001-A0899 and 1434-HQ-97AG01718. The SCEC contribution number for this paper is 706. This work was also supported by NEHRP/USGS Grant 01HQER0183.

References

Ben-Zion, Y., and P. E. Malin (1991). San Andreas fault zone head waves near Parkfield, California, *Science* **251,** 1592–1594.

Bonilla, L. F., J. H. Steidl, G. T. Lindley, A. G. Tumarkin, and R. J. Archuleta (1997). Site amplification in the San Fernando Valley, California: variability of site-effect estimation using the *S*-wave, coda, and H/V methods, *Bull. Seism. Soc. Am.* **87,** 710–730.

Ebel, J. (1989). The effect of crustal scattering on observed high-frequency earthquake seismograms, *Geophys. J. R. Astr. Soc.* **98,** 329–341.

Ebel, J. E., and K. P. Bonjer (1990). Moment tensor inversion of small earthquakes in southwestern Germany for the fault plane solution, *Geophys. J. Int.* **101,** 133–146.

Hardebeck, J. L., and P. M. Shearer (2002). A new method for determining first-motion focal mechanisms, *Bull. Seism. Soc. Am.* **92,** 2264–2276.

Hauksson, E. (2000). Crustal structure and seismicity distribution adjacent to the Pacific and North America plate boundary in southern California, *J. Geophys. Res.* **105,** 13,875–13,903.

Hauksson, E., and J. S. Haase (1997). Three-dimensional V_p and V_p/V_s velocity models of the Los Angeles Basin and central Transverse Ranges, California, *J. Geophys. Res.* **102,** 5423–5453.

Jennings, C. W. (1975). Fault map of California with locations of volcanoes, thermal springs, and thermal wells, California Division of Mines and Geology, scale 1:750,000.

Julian, B. R., and G. R. Foulger (1996). Earthquake mechanisms from linear-programming inversion of seismic-wave amplitude ratios, *Bull. Seism. Soc. Am.* **86,** 972–980.

Kilb, D., J. Hardebeck, A. Hindley, P. Shearer, J. Eakins, and F. Vernon (2002). Waveform and focal mechanism heterogeneity in aftershocks of the 10/31/2001 *M*5.1 Anza, California, earthquake: why and where, in *The 2002 SCEC Annual Meeting* (Proceedings and Abstracts), p. 86.

Kisslinger, C. (1980). Evaluation of *S* to *P* amplitude ratios for determining focal mechanisms from regional network observations, *Bull. Seism. Soc. Am.* **70,** 999–1014.

Kisslinger, C., J. R. Bowman, and K. Koch (1981). Procedures for computing focal mechanisms from local $(SV/P)_2$ data, *Bull. Seism. Soc. Am.* **71,** 1719–1729.

Nakamura, A., S. Horiuchi, and A. Hasegawa (1999). Joint focal mechanism determination with source-region station corrections using short-period body-wave amplitude data, *Bull. Seism. Soc. Am.* **89,** 373–383.

Rau, R.-J., F. T. Wu, and T.-C. Shin (1996). Regional network focal mechanism determination using 3D velocity model and *SH*/*P* amplitude ratio, *Bull. Seism. Soc. Am.* **86,** 1270–1283.

Reasenberg, P., and D. Oppenheimer (1985). FPFIT, FPPLOT, and FPPAGE: FORTRAN computer programs for calculating and displaying earthquake fault-plane solutions, *U.S. Geol. Surv. Open-File Rept. 85-739*, 109 pp.

Richards-Dinger, K. B., and P. M. Shearer (2000). Earthquake locations in southern California obtained using source-specific station terms, *J. Geophys. Res.* **105,** 10,939–10,960.

Rögnvaldsson, S. T., and R. Slunga (1993). Routine fault plane solutions for local networks: a test with synthetic data, *Bull. Seism. Soc. Am.* **83,** 1232–1247.

Schwarz, S. Y. (1995). Source parameters of aftershocks of the 1991 Costa Rica and 1992 Cape Mendocino, California, earthquakes from inversion of local amplitude ratios and broadband waveforms, *Bull. Seism. Soc. Am.* **85,** 1560–1575.

Shearer, P. M. (1997). Improving local earthquake locations using the L1 norm and waveform cross correlation: application to the Whittier Narrows, California, aftershock sequence, *J. Geophys. Res.* **102,** 8269–8283.

Shearer, P. M. (1999). *Introduction to Seismology*, Cambridge U Press, New York, 260 pp.

Shearer, P. M., J. L. Hardebeck, L. Astiz, and K. B. Richards-Dinger (2003). Analysis of similar event clusters in aftershocks of the 1994 Northridge, California, earthquake, *J. Geophys. Res.* **108,** no. B1, 2035, doi 10.1029/2001JB000685.

Shen, Y., D. W. Forsyth, J. Conder, and L. M. Dorman (1997). Investigation of microearthquake activity following an intraplate teleseismic swarm on the west flank of the southern East Pacific Rise, *J. Geophys. Res.* **102,** 459–475.

Institute of Geophysics and Planetary Physics
Scripps Institution of Oceanography
University of California, San Diego
La Jolla, California 92093

Manuscript received 27 November 2002.